Effect of Chirped Gratings on Reflective Optical Bistability in DFB Semiconductor Laser Amplifiers

Drew N. Maywar, *Student Member, IEEE,* and Govind P. Agrawal, *Fellow, IEEE*

***Abstract*— We use spatial chirp of the built-in grating to improve optical bistability on reflection from distributed feedback semiconductor laser amplifiers. We show that improvements in the on–off switching ratio occur because spatial chirp greatly affects the saturation behavior of the reflectivity resonances, allowing access to states of low reflection during bistable switching. We also show that spatial chirp modifies the spectral range of the variety of hysteresis shapes that occur on reflection. In doing so, we discover a new type of hysteresis loop that reveals a qualitative difference between the loop-shaped hystereses occurring near the two edges of the stop band. With spatial chirp, the new hysteresis loop can exhibit an on–off switching ratio in excess of 100 000.**

***Index Terms*— Amplifiers, distributed feedback devices, gratings, optical bistability, optical switches.**

I. Introduction

OPTICAL bistability in semiconductor laser amplifiers (SLA's) is well suited for applications in optical switching [1], [2], signal processing [3], [4], memory [5], [6], and logic [7]. SLA's are compact ($\sim$300 μm^3 active volume), are capable of monolithic integration in photonic circuits, provide amplification, and can be fabricated to operate at any wavelength used in optical communications [8]. Their strong nonlinearity and inherent gain lead to switching at microwatt levels with switching times less than one nanosecond, resulting in femtojoule switching energies [9].

In a distributed feedback (DFB) device, bistability is supported by feedback provided by a built-in diffraction grating [10], [11]. Gratings are especially useful as feedback elements in single-substrate photonic circuits because integration can be achieved without requiring facets. The bistable performance of a DFB device can be improved by varying the spatial frequency of the grating (referred to as spatial chirp). For example, spatial chirp can lower the optical signal power required for switching, as was shown for passive devices exhibiting a Kerr-type nonlinearity [12], [13]. In $\lambda/4$-shifted DFB SLA's, spatial chirp increases the spectral range of low-threshold switching [14]. These investigations, though, focus on transmissive bistability.

Reflection from DFB SLA's, unlike transmission, exhibits a variety of bistable hysteresis shapes [15], each with its own switching behavior. This diversity increases the potential applications of bistable DFB SLA's. The objective of this paper is to show how spatial chirp can improve these reflective hystereses. We will focus in particular on modifications in the spectral range of such hystereses and on improvements to the on–off switching ratios.

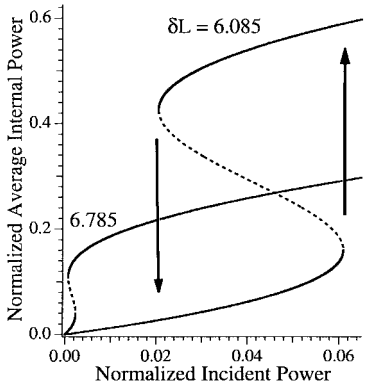

Fig. 1. Average-internal-power hystereses for two signal wavelengths. The longer signal wavelength [$\delta L = 6.085$ via (5)] exhibits higher switching thresholds. Other parameters are: $\alpha = 5$, $\kappa L = 3$, $g_o L = 1.198\,15$, and $\alpha_{int} L = 0$. The powers are normalized to the saturation power (typically 10 mW). Dashed portions of the curves are unstable.

The paper is organized as follows. In the next section, we discuss the positive feedback loop that gives rise to optical bistability and outline our computational model. In Section III, we discuss the variety of reflective hysteresis shapes in terms of the saturation behavior of reflectivity resonances. During this discussion, we demonstrate a new hysteresis loop on reflection from DFB SLA's. In Section IV, we show how spatial chirp affects reflective bistability by changing the saturation behavior of the reflectivity resonances. We focus on the cases exhibiting high on–off switching ratios and show that values greater than 100 000 can be obtained using the new hysteresis loop.

II. Optical Bistability in DFB SLA's

A. Physical Process

Optical bistability is characterized by a steady-state hysteresis, as shown in Fig. 1. Here, the average internal optical power is plotted as a function of the incident power for two signal wavelengths. For each hysteresis, two regions of stable

Manuscript received May 5, 1998. This work was supported in part by the U.S. Department of Education and the National Science Foundation.

The authors are with The Institute of Optics and Rochester Theory Center, University of Rochester, Rochester, NY 14627 USA.

Publisher Item Identifier S 0018-9197(98)08874-5.

power (solid lines) are connected by a region of instability (dashed line). The internal power switches between the two stable branches by means of a positive feedback loop occurring for the optical power within the DFB SLA.

The positive feedback loop for dispersive optical bistability requires two ingredients: a cavity resonance and an intensity-dependent refractive index. In SLA's, the latter arises from the dependence of the refractive index on the carrier density [8]. An optical signal that depletes the carrier density by stimulated emission (i.e., gain saturation) simultaneously increases the refractive index.

In DFB SLA's, a built-in diffraction grating provides feedback along the length of the amplifier, and therefore creates an effective cavity even without facet mirrors. Cavity resonances (localized spectral regions of high internal power) occur at both edges of the stopband (a spectral region of low transmission centered at the Bragg wavelength).

Optical switching occurs via the following positive feedback loop. An optical signal enters the amplifier with a center wavelength longer than that of a cavity resonance. An increase in the optical power within the amplifier increases the refractive index, and the stopband (and cavity resonance) shifts to longer wavelengths. If the cavity resonance moves onto the signal wavelength, the internal optical power increases more. As a result, the refractive index continues to increase, and the stopband shifts to even longer wavelengths. This positive feedback loop for the internal power moves the cavity resonance fully onto the signal wavelength. The resulting jump experienced by the internal power is indicated by the up-arrow in Fig. 1.

The reverse process occurs at the down-arrow. If the incident power is lowered so that the signal wavelength is at the peak of the cavity resonance, a small subsequent decrease in incident power will initiate the reverse positive feedback loop. In this case, the cavity resonance shifts away from the signal wavelength, and internal power switches downward. These two switching processes give rise to the common S-shaped hysteresis.

The two bistability curves shown in Fig. 1 exhibit different switching threshold powers. The optical signal with the longer wavelength ($\delta L = 6.085$) is initially farther away from the cavity resonance and therefore requires a larger incident power to seed the positive feedback loop. The correspondingly larger internal power and higher gain saturation for longer wavelength signals greatly affect the shape of the hysteresis on reflection, as discussed later in Section III.

B. Computational Analysis

Optical bistability in DFB SLA's can be studied using the following model. The optical field is expressed as

$$E(z) = A(z)\,\exp(i\beta_B z) + B(z)\,\exp(-i\beta_B z) \tag{1}$$

where A and B are the slowly varying envelopes of the forward- and backward-propagating fields, respectively. The Bragg wavenumber β_B is given by

$$\beta_B = \frac{2\pi n}{\lambda_B} = \frac{\pi}{\Lambda} \tag{2}$$

where n is the average refractive index associated with the fundamental waveguide mode, the parameter $\lambda_B (= 2n\Lambda)$ is the Bragg wavelength, and Λ is the period of the built-in grating.

The field distribution inside the DFB SLA can be calculated via the standard coupled-mode equations [14]

$$\frac{dA}{dz} = \left[i\delta + \frac{g}{2}(1 - i\alpha) - \frac{\alpha_{\text{int}}}{2}\right]A + i\kappa B \tag{3}$$

$$-\frac{dB}{dz} = \left[i\delta + \frac{g}{2}(1 - i\alpha) - \frac{\alpha_{\text{int}}}{2}\right]B + i\kappa A. \tag{4}$$

Here, κ is the coupling coefficient, α_{int} accounts for internal losses, and g is the gain coefficient. The linewidth enhancement factor α represents the coupling between the refractive index and optical gain that occurs in semiconductor gain media.

The detuning parameter δ in the coupled-mode equations is given by

$$\delta = \beta - \beta_B = \frac{2\pi n_o}{\lambda_o} - \frac{\pi}{\Lambda} \tag{5}$$

where β and n_o are the carrier-density-independent parts of the signal wavenumber and the spatially averaged modal refractive index, respectively. [The carrier-density-dependent contribution to the detuning is represented by the $-(g/2)\alpha$ term in (3) and (4).] The detuning δ is related to the free-space signal wavelength λ_o such that, for constant n_o and Λ, smaller values of detuning correspond to longer signal wavelengths.

The gain coefficient for CW signals and pulses much wider than the semiconductor carrier lifetime τ_c ($\sim$100 ps) is given by [14]

$$g = \frac{g_o}{1 + \overline{P}}. \tag{6}$$

Here, g_o is the small-signal gain, which we assume is flat over the spectral range near the stopband ($\sim$1 nm). The quantity $\overline{P} = P/P_{\text{sat}}$ is the optical power normalized to the saturation power $P_{\text{sat}} = \sigma hc/(\lambda_o \tau_c a)$, where h is Planck's constant and c is the speed of light in vacuum. A typical value of P_{sat} is 10 mW, if we use $\sigma = 0.4\ \mu\text{m}^2$ for the transverse area of the optical mode, $\lambda_o = 1.55\ \mu$m for the operating wavelength, $\tau_c = 200$ ps for the carrier lifetime, and $a = 2.5 \times 10^{-16}$ cm^2 for the differential gain. In terms of the field envelopes, the normalized power is given by

$$\overline{P}(z) = \frac{|E(z)|^2 \Gamma\sigma}{P_{\text{sat}}} \approx \frac{[|A(z)|^2 + |B(z)|^2]\Gamma\sigma}{P_{\text{sat}}} \tag{7}$$

where the confinement factor Γ represents the fraction of the optical power of the transverse mode within the active region. The effect of the neglected optical interference term (with a period of $\sim$0.2 μm) is assumed to be washed out by carrier diffusion (typical diffusion length $\sim$2 μm).

We solve this set of nonlinear equations via a transfer-matrix method [16] that divides the amplifier into many small sections. Transfer matrices, corresponding to each section, are calculated from the analytic solutions [14] to a linearized form of (3) and (4). The power values along the amplifier are used to saturate the gain in each region, after which the power profile is recalculated. This iteration procedure is continued until

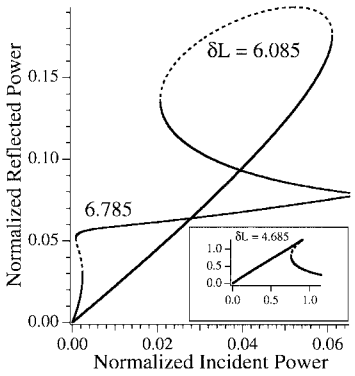

Fig. 2. Reflected-power hysteresis shapes under conditions identical to those of Fig. 1. The inset shows a hysteresis for an even longer signal wavelength. All signal wavelengths are on the short-wavelength side of the stopband. Where the stable branches (solid lines) become unstable, the reflected power switches to the other stable branch at the same incident power.

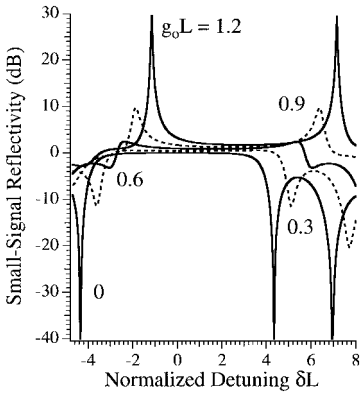

Fig. 3. Evolution of the small-signal reflectivity spectrum with change in gain for the parameter values of Fig. 1. Reflectivity resonances at the stopband edges reshape from a peak to a dip, and shift to longer signal wavelengths, as gain is decreased.

convergence (we refer the reader to [14] for further details). Although neglected in this paper, finite facet reflectivities may be included using appropriate matrices [17].

III. Uniform-Grating DFB SLA's

Although the hysteresis curves for the average internal power in Fig. 1 are both S-shaped, the corresponding reflected-power hystereses take on different shapes, as shown in Fig. 2 for the same signal wavelengths used in Fig. 1. While the hysteresis for the shorter wavelength ($\delta L = 6.785$) is S-shaped, the longer wavelength signal exhibits a loop-shaped hysteresis. A third hysteresis shape, for an even longer wavelength ($\delta L = 4.685$), is given in the inset.

Each reflective hysteresis shares the same switching threshold powers as its corresponding average-internal-power hysteresis. The unstable region, which connects these thresholds, can therefore be determined straightforwardly. The switching thresholds are the same because reflective bistability is supported by the *same* positive feedback loop described in Section II—i.e., a positive feedback loop involving the intensity-dependent refractive index, a cavity resonance, and the signal's *internal* power.

The shape of each reflected-power hysteresis can be understood in terms of differences between the cavity resonance supporting the bistable switching and a *reflectivity* resonance. By reflectivity resonance, we mean a localized spectral region of either high or low reflectivity. This region may be centered at a different wavelength than, or may have a different spectral width than, the corresponding cavity resonance. These differences depend, in part, on the coupling strength induced by the built-in grating (we use $\kappa L = 3$ throughout this paper) and on which side of the stopband the particular cavity resonance occurs. Differences between the reflectivity and cavity resonance also depend on the amount of *gain* within the DFB SLA—a feature that does not (necessarily) exist for switching devices based on a passive $\chi^{(3)}$ nonlinearity. We will illustrate how the reflectivity resonances depend on gain by examining the small-signal regime.

For small optical powers (<0.1 μW), saturation can be ignored, and the reflectivity resonances exhibit the following dependence on gain. For large amounts of gain (enough to approach lasing threshold), reflectivity resonances occur as peaks at both edges of the stopband, as seen in Fig. 3 for $g_oL = 1.2$. As the gain is decreased, the reflectivity peaks begin to disappear, and dips arise at wavelengths slightly farther away from the stopband. This reshaping of the reflectivity resonances is apparent in Fig. 3 for $g_oL = 0.6$. With less gain, the peaks completely disappear and the dips push downward. For $g_oL = 0$ (the case of passive filters), the reflectivity resonances are deep dips. The red shift of the stopband with decreasing gain results from the corresponding increase in the refractive index.

The small-signal reflectivity resonance behavior of Fig. 3 is helpful in understanding the reflected-hysteresis shapes because bistable switching is accompanied by gain saturation. The amount of saturation depends on the initial detuning of the signal wavelength from the cavity resonance, as mentioned in Section II. Consequently, different spectral regions will have different reflective hysteresis shapes.

For signal wavelengths initially tuned close to a cavity resonance, a low internal power is required to seed optical bistability. The relatively low internal power during the positive feedback loop allows the gain to remain relatively high under saturation. Thus, the reflectivity resonance is a peak during the positive feedback loop. Moreover, we find (using the saturated gain profile) that the reflectivity resonance spectrally overlaps the cavity resonance, which is also shaped like a high peak. Since the cavity and reflectivity resonances are similar, the reflected power switches in the same manner, as evident by the S-shaped hysteresis of Fig. 2. After upward switching, the on-state of this hysteresis exhibits about 13-dB amplification.

In contrast, signal wavelengths initially tuned far from the cavity resonance require higher optical powers to seed the positive feedback loop. The correspondingly large internal powers saturate the gain enough that the reflectivity resonance is a dip during the switching process. As the reflectivity resonance shifts to longer wavelength, the reflected signal power drops accordingly. Thus, the reflected power switches downward even though the average internal power switches

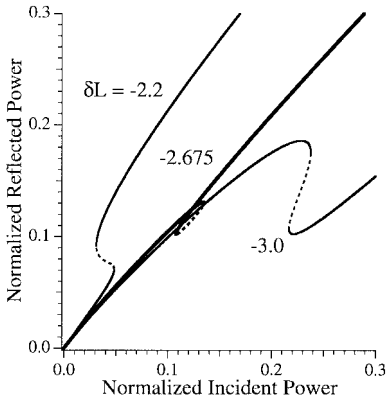

Fig. 4. Bistable behavior of the reflected power for three signal wavelengths on the *long*-wavelength edge of the stopband for the same device used in Fig. 1. The middle curve is a new hysteresis shape—a loop that occurs below the stable branches.

upward. This behavior gives rise to an inverted-S-shaped hysteresis, like the one in the inset of Fig. 2. The on-state typically exhibits no amplification since the gain is strongly saturated. Notice that the high-incident-power tail of this hysteresis pushes down beyond the switching thresholds. The signal is simply experiencing the growing reflectivity dip.

The remaining hysteresis of Fig. 2 is shaped like a loop. The top of the loop is unstable and switching occurs down from both sides [15] from on-states of a few decibels in amplification. Loop-shaped hysteresis occur in a spectral range between the hysteresis described above. For these signal wavelengths, the internal powers saturate the gain to levels where the cavity resonance is reshaping from a peak to a dip (see $g_oL = 0.6$ in Fig. 3). The reflectivity peak and dip straddle the central wavelength of the cavity resonance, with the peak slightly closer to the stopband.

For reflection from the short-wavelength edge of the stopband, the reflectivity resonance peak occurs at a longer wavelength than the cavity resonance. The peak may therefore completely pass through the signal wavelength, resulting in an increase and then decrease in the reflected power. This kind of a mismatch between the internal and output resonances was shown to gives rise to loop-shaped hysteresis in other geometries as well [18], [19]. For DFB SLA's, downward switching on the high-incident-power side of the hysteresis is facilitated by the reflectivity resonance dip. As the stopband shifts to longer wavelengths, this dip shifts toward the optical signal. Moreover, gain saturation during the positive feedback loop will push the dip to lower values of reflectivity while quenching the resonance peak.

An interesting feature of the loop-shaped hysteresis is that its shape is qualitatively different for reflection at either edge of the stopband. On the long-wavelength edge, the loop occurs predominantly *under* the stable-power branches. The bottom portion of the loop is unstable and upward switching occurs at both sides, as shown in Fig. 4. Here, we have left out the spectral evolution of the loop hysteresis to focus on the loop at $\delta L = -2.675$. During the transition from one hysteresis shape to another, upward and downward switching may occur, in general, on either side of loop-shaped hysteresis.

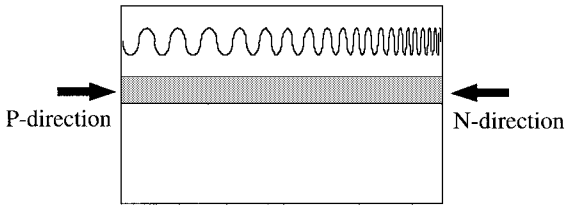

Fig. 5. Schematic illustration of a DFB SLA with a linearly chirped grating, indicating the P-direction ($C > 0$) and N-direction ($C < 0$).

The origin of such a loop may be understood as follows. For reflection from the long-wavelength edge of the stopband, the reflectivity resonance peak and dip straddle the central wavelength of the cavity resonance with the *dip* at the longer wavelength. Therefore, as the stopband shifts to longer wavelengths, the optical signal is affected first by the reflectivity dip and then the peak. Consequently, the reflected signal decreases and then increases, giving rise to the particular shape of the hysteresis loop. In our calculations for Fig. 4, we find that even though the bottom of the reflectivity dip is not reached, the reshaping of the reflectivity resonance is enough to initially pull the reflected power down. The resulting on–off switching ratios are small. Moreover, since the summit of the reflectivity peak is not encountered, large amplification is not realized.

To our knowledge, this is the first report of qualitatively different hysteresis loops occurring at either edge of the DFB SLA stopband. The loop on the long-wavelength edge may have gone unnoticed since its on–off switching ratios can be quite small. This new hysteresis loop, though, is intriguing because it occurs predominantly below the stable reflected-power branches and points toward zero reflected power. One may be able to design a device for which the loop approaches zero reflected power, making the on–off switching ratio very large. This will occur if the signal wavelength encounters a deep reflectivity dip. In the following section, we pursue this idea by introducing spatial chirp into the built-in diffraction grating.

IV. Chirped-Grating DFB SLA's

A DFB SLA with a linearly chirped grating is depicted in Fig. 5. The P-direction is defined to be the direction for which an incident optical field sees an *increase* in the spatial frequency (and Bragg wavenumber) of the grating. Likewise, an optical field incident in the N-direction sees, by definition, a decrease in the spatial frequency of the grating. ("P" and "N" indicate positive and negative chirp, respectively, in our notation.)

The P- or N-direction is specified in computations by the sign of the chirp parameter C, introduced by using

$$\beta_B(z) = \overline{\beta}_B + C\frac{(z - L/2)}{L^2} \tag{8}$$

where $\overline{\beta}_B$ is the average Bragg wavenumber. A positive (negative) value of C corresponds to the P-direction (N-direction), and the magnitude of C represents the total change in $\beta_B(z)L$ along the device. For small amounts of spatial chirp, the coupled-mode equations (3) and (4) remain unchanged except

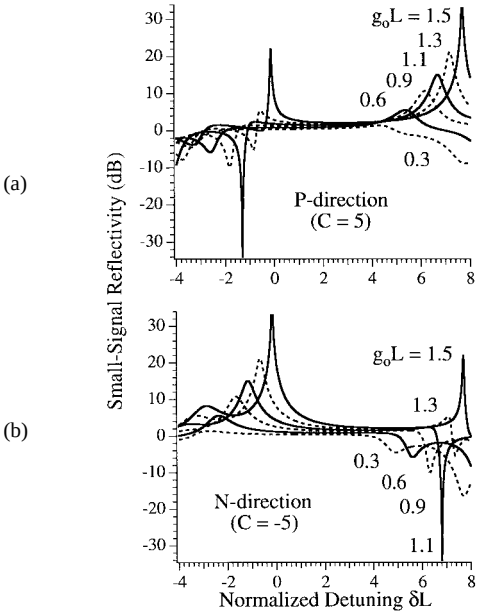

Fig. 6. Small-signal reflectivity spectra for several values of the gain for an optical signal incident in the (a) P-direction and (b) N-direction of a linearly chirped-grating DFB SLA with $|C| = 5$. Other parameters are: $\alpha = 5$, $\kappa L = 3$, and $\alpha_{\rm int} L = 0$. Note how a deep reflectivity dip can be realized near one edge of the stopband for a relatively high value of gain ($gL = 1.1$).

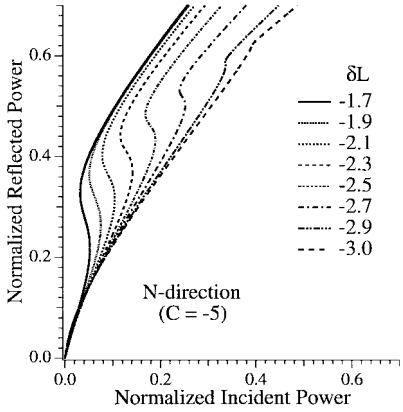

Fig. 7. Spectral evolution of the reflected-power hysteresis for optical signals incident in the N-direction near the long-wavelength-edge of the stopband. Parameters are the same as in Fig. 6, except that $g_oL = 1.5081$. The inverted-S- and loop-shaped hysteresis do not occur (compare with Fig. 4).

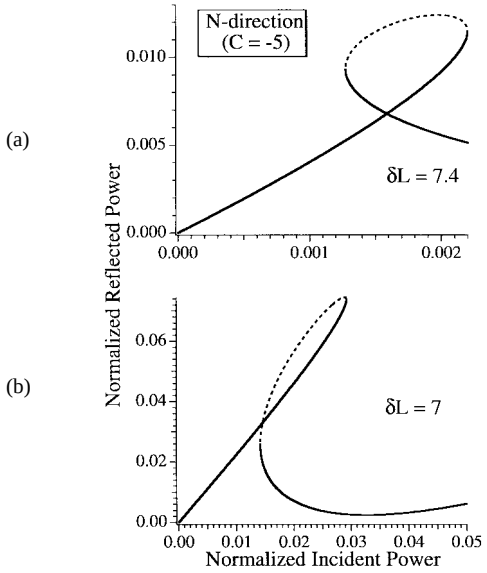

Fig. 8. Reflected-power hysteresis for optical signals incident in the N-direction with wavelengths on the short-wavelength side of the stop band. All other parameters are the same as in Fig. 7. (a) The switching thresholds for the loop-shaped hysteresis are an order of magnitude smaller than those of Fig. 2. (b) The on–off switching ratio exceeds 30 for the high-incident-power side of the hysteresis.

that the detuning parameter $\delta = \beta - \beta_B$ now becomes z dependent. In this section, we use a value of $|C| = 5$, which corresponds to a total variation in β_B of about 0.1% for a 300-μm-long device.

Spatial chirp has a major effect on reflective bistability in DFB SLA's because it changes the saturation behavior of the reflectivity resonances. To illustrate this change, it is (again) instructive to examine the small-signal regime. For optical signals incident in either the P-direction or the N-direction, reflections from the two edges of the stopband exhibit remarkably different behavior, as seen by the reflectivity spectra shown in Fig. 6.

Reflectivity resonances exhibit peaks in spite of a reduction in gain for short-wavelength signals incident in the P-direction [Fig. 6(a)] and for long-wavelength signals incident in the N-direction [Fig. 6(b)]. Each of these signals has a wavelength that matches the Bragg wavelength away from the input facet and therefore travels deep into the amplifier before being reflected. The increased gain–length product results in the enhanced reflection [20].

For these two enhanced-reflection cases, we find that the reflectivity resonances remain spectrally overlapped with the cavity resonances. As a result, the reflected-power behavior mimics that of the internal power, and only S-shaped hysteresis occur. Fig. 7 shows the spectral evolution of reflective bistability at the long-wavelength edge of the stopband for optical signals incident in the N-direction. The inverted-S- and loop-shaped hysteresis do not appear at all.

In contrast, an *increase* in spectral range for inverted-S- and loop-shaped hysteresis occurs for each optical signal with a wavelength that matches the Bragg wavelength near the *input* facet of the DFB SLA. This condition is satisfied for long-wavelength signals incident in the P-direction [Fig. 6(a)] and for short-wavelength signals incident in the N-direction [Fig. 6(b)]. Here, the reflectivity resonance peak readily diminishes with gain saturation. Moreover, we find that the reflectivity resonance dip is the most prominent for a *nonzero* value of gain. In Fig. 6, large reflectivity dips occur for $g_oL = 1.1$. Increasing the amount of spatial chirp tends to increase the value of gain for which the dip is most prominent. Gain saturation via the optical signal now has an even larger effect on the reflected-power hysteresis.

A consequence of the above behavior is that loop-shaped hystereses occur at smaller incident powers. Fig. 8(a) shows a loop-shaped hysteresis for an optical signal on the short-wavelength edge of the stopband, incident in the N-direction of a chirped-grating DFB SLA. The hysteresis is similar in shape to that of Fig. 2, but the switching powers are one order of

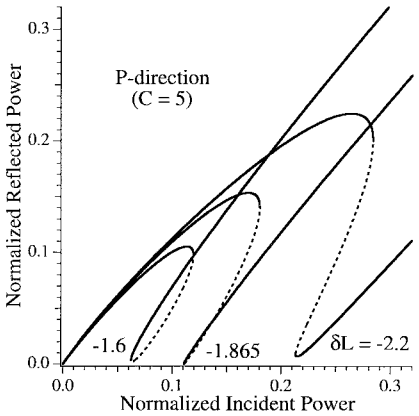

Fig. 9. Reflected-power hysteresis for signals incident in the P-direction with wavelengths on the long-wavelength edge of the stop band. All other parameters are the same as in Fig. 7. The on–off switching ratio exceeds 100 000 for the low-incident-power side of the middle hysteresis.

magnitude smaller. (For both cases, the small-signal gain is set at about 95% of lasing threshold.) For a device with $P_{\rm sat} = 10$ mW, this corresponds to 20-μW switching. The loop-shaped hystereses not only occur for smaller incident powers, but also exist over a wider spectral range than for the unchirped case.

As discussed in Section III, the high-incident-power tail of the reflected-power hysteresis pushes down for signal wavelengths on the short-wavelength side of the stopband. For the chirped-grating case, a deep reflectivity dip can affect the optical signal during the bistable switching process, allowing the bottom of the hysteresis tail to approach zero reflected power. An example is given in Fig. 8(b), for a longer optical wavelength than in Fig. 8(a). Downward switching occurs from an on-state of about 4-dB amplification with an on–off switching ratio of about 30.

For the *long*-wavelength side of the stopband, a deep reflectivity dip may also be experienced by the optical signal during the positive feedback loop. This causes the hysteresis loop to push down toward zero for the loop- and inverted-S-shaped hysteresis, as shown in Fig. 9 for signals incident in the P-direction. The on–off switching ratios at the low-incident-power side are greater than 30 for the outer hysteresis, which span a spectral range of $\delta L = 0.6$. This corresponds to a spectral width of about 27 GHz for a 300-μm-long device operating near 1.55 μm. Within this spectral region, the reflective hysteresis obtains an on–off switching ratio in excess of 100 000, as exhibited by the middle hysteresis of Fig. 9. In spite of these excellent switching ratios, amplification has been lost since the peaked-reflectivity resonance is not encountered by the optical signal.

V. Conclusion

DFB SLA's support reflectivity resonances that range from high-amplification peaks to zero-reflection dips, depending on the amount of gain. Gain saturation can therefore reshape reflectivity resonances from one extreme to the other. This reshaping gives rise to a wide variety of reflected-power hysteresis, mainly because of differences between the reflectivity and cavity resonances. The loop-shaped and inverted-S-shaped hysteresis are intriguing because the reflectivity resonance dip is involved in the bistable switching process. The lower the reflectivity dip, the higher the on–off switching ratio.

By introducing spatial chirp into the built-in grating, the reflectivity resonance can push toward zero reflectivity during the bistable switching process. This occurs for signal wavelengths that match the Bragg wavelength near the input facet of a chirped-grating DFB SLA. For $|C| = 5$, we found optical wavelengths for which the on–off switching ratio exceeds 30 at one side of their reflected-power hysteresis. For the N-direction, this high switching ratio is accompanied by an on-state of about 4-dB amplification. For the P-direction, an on–off switching ratio of at least 30 is realized for optical signals over a spectral range of about 27 GHz, with the maximum switching ratio exceeding 100 000, but without amplification.

Ideally, large on-state amplification will coexist with improvements in the on–off switching ratio. This will occur if the optical signal experiences both a high-reflectivity peak and a low-reflectivity dip during the bistable switching process. Such behavior may be achieved by optimizing parameters such as the coupling strength, the linewidth enhancement factor, and the chirp parameter. In addition, other grating nonuniformities (including different chirp profiles), nonzero facet reflectivities, and resonances away from the stopband edges may also contribute to high-contrast high-gain switching. We are currently investigating some of these options.

Acknowledgment

The authors are grateful to J. R. Marciante and G. H. M. van Tartwijk for fruitful discussions.

References

[1] H. Kawaguchi, "Progress in optical functional devices using two-section laser diodes/amplifiers," *Proc. Inst. Elect. Eng.,* pt. J, vol. 140, pp. 3–15, 1993.

[2] M. Dagenais and W. F. Sharfin, "Bistable diode laser amplifiers in high performanceoptical communication and optical computing systems," *Proc. SPIE,* vol. 881, pp. 80–91, 1988.

[3] N. Ogasawara and R. Ito, "Static and dynamic properties of nonlinear semiconductor lasers amplifiers," *Jpn. J. Appl. Phys.,* vol. 25, pp. 739–742, 1986.

[4] R. P. Webb, "Error-rate measurements on an all-optically regenerated signal," *Opt. Quantum Electron.,* vol. 19, pp. S57–S60, 1987.

[5] K. Inoue, "All-optical flip-flop operation in an optical bistable device using two lights of different frequencies," *Opt. Lett.,* vol. 12, pp. 918–920, 1987.

[6] S. D. Smith, "Optical circuits," in *Optical Computing,* B. S. Wherrett and F. A. P. Tooley, Eds. New York: Edinburgh Univ., 1989, ch. 6.

[7] W. F. Sharfin and M. Dagenais, "High contrast, 1.3 mm optical and gate with gain," *Appl. Phys. Lett.,* vol. 48, pp. 1510–1512, 1986.

[8] G. P. Agrawal and N. K. Dutta, *Semiconductor Lasers,* 2nd ed. New York: Van Nostrand Reinhold, 1993.

[9] W. F. Sharfin and M. Dagenais, "Femtojoule optical switching in nonlinear semiconductor laser amplifiers," *Appl. Phys. Lett.,* vol. 48, pp. 321–322, 1986.

[10] H. G. Winful, J. H. Marburger, and E. Garmire, "Theory of bistability in nonlinear distributed feedback structures," *Appl. Phys. Lett.,* vol. 35, pp. 379–381, 1979.

[11] M. J. Adams and R. J. Wyatt, "Optical Bistability in distributed feedback semiconductor laser amplifiers," *Proc. Inst. Elect. Eng.,* pt. J, vol. 134, pp. 35–40, 1987.

[12] G. Assanto and R. Zanoni, "Almost-periodic nonlinear distributed feedback gratings," *Opt. Acta,* vol. 34, pp. 89–101, 1987.

[13] J. Liu, C. Liao, S. Liu, and W. Xu, "The dynamics of direction-dependent switching in nonlinear chirped gratings," *Opt. Commun.*, vol. 130, pp. 295–301, 1996.
[14] D. N. Maywar and G. P. Agrawal, "Transfer-matrix analysis of optical bistability in DFB semiconductor laser amplifiers with nonuniform gratings," *IEEE J. Quantum Electron.*, vol. 33, pp. 2029–2037, 1997.
[15] M. J. Adams, "Optical amplifier bistability on reflection," *Opt. Quantum Electron.*, vol. 19, pp. S37–S45, 1987.
[16] M. Yamada and K. Sakuda, "Analysis of almost-periodic distributed feedback slab waveguides via a fundamental matrix approach," *Appl. Opt.*, vol. 26, pp. 3474–3478, 1987.
[17] R. Hui and A. Sapia, "Nonlinearity difference in the two passbands of a distributed-feedback semiconductor laser amplifier," *Opt. Lett.*, vol. 15, pp. 956–958, 1990.
[18] A. D. Lloyd, I. Janossy, H. A. Mackenzie, and B. S. Wherrett, "CW optical bistability in nonabsorbing liquids and liquid crystals," *Opt. Commun.*, vol. 61, pp. 339–344, 1987.
[19] D. C. Hutchings, A. D. Lloyd, I. Janossy, and B. S. Wherrett, "Theory of optical bistability in metal-mirrored Fabry–Perot cavities containing thermo-optic materials," *Opt. Commun.*, vol. 61, pp. 345–350, 1987.
[20] M. Yamada and K. Sakuda, "Adjustable gain and bandwidth light amplifiers in terms of distributed feedback structures," *J. Opt. Soc. Amer. A*, vol. 4, pp. 69–76, 1987.

Drew N. Maywar (S'97) was born in Port Huron, MI, on March 1, 1970. He received the B.S. degree in optics and the B.A. degree with honors in religion in 1993, and the M.S. degree in optics in 1997, all from the University of Rochester, Rochester, NY. He is currently working toward the Ph.D. degree in optics on the topic of optical switching and bistability in distributed feedback semiconductor optical amplifiers at the same university.

In 1991, he spent a year at the Center for Japanese Studies, Nanzan University, Japan. From 1993 to 1994, he was a Fulbright Scholar at Osaka University's Institute of Laser Engineering, Osaka, Japan, where he studied the temperature dependence of gain in Nd : glass laser amplifiers.

In October of 1998, he began part of his doctoral research at the University of Tokyo under the auspices of the National Science Foundation's Dissertation Enhancement Award.

Govind P. Agrawal (M'83–SM'86–F'96) received the B.S. degree from the University of Lucknow in 1969 and the M.S. and Ph.D. degrees from the Indian Institute of Technology, New Delhi, India, in 1971 and 1974, respectively.

After holding positions at the Ecole Polytechnique, France, the City University of New York, NY, and AT&T Bell Laboratories, Murray Hill, NJ, he joined the faculty of the Institute of Optics at the University of Rochester in 1989, where he is a Professor of Optics. His research interests focus on quantum electronics, nonlinear optics, and laser physics. In particular, he has contributed significantly to the fields of semiconductor lasers, nonlinear fiber optics, and optical communications. He is an author or co-author of more than 250 research papers, several book chapters, and review articles, and three books entitled *Semiconductor Lasers* (New York: Van Nostrand Reinhold, 1993), *Nonlinear Fiber Optics* (New York: Academic, 1995), and *Fiber-Optic Communication Systems* (New York: Wiley, 1997). He has also edited the books *Contemporary Nonlinear Optics* (New York: Academic, 1992) and *Semiconductor Lasers: Past, Present and Future* (Woodbury, NY: AIP Press, 1995).

Dr. Agrawal is a fellow of the Optical Society of America.